scientific reports

Check for updates

OPEN

Glucose-functionalized gold nanoparticles for effective photothermal therapy in lung cancer

Juan Braga Menendez[1,2], Mariel Fusco[1], Flavia Piccioni[1], Constanza Arriola Benitez[1], Manglio Miguel Rizzo[1,3], Patrizia Andreozzi[4], Sergio E. Moya[5], M. Fernanda Cardinal[6,7]✉ & Mariana Malvicini[1,7]✉

Lung cancer remains the leading cause of cancer-related mortality worldwide, largely due to late-stage diagnoses that severely limit therapeutic interventions. In this context, nanoparticle-mediated photothermal therapy (PTT) has emerged as a promising and minimally toxic modality for solid tumors. We synthesized gold nanoparticles (AuNPs) with three distinct morphologies—spheres, rods, and stars—and functionalized them with polyethylene glycol (AuNPs-PEG) or polyethylene glycol conjugated with 2-deoxy-D-glucose (AuNPs-Gluc). In vitro analyses using human (A549, H1299) and murine (LLC) lung carcinoma cell lines demonstrated that PEGylation significantly attenuated AuNP-associated cytotoxicity, while glucose functionalization further enhanced biocompatibility. Inductively coupled plasma mass spectrometry quantification confirmed superior cellular uptake of AuNPs-Gluc compared to AuNPs-PEG ($p < 0.05$). Subsequent irradiation with a 980 nm diode laser (1 W) induced robust thermal damage and apoptotic cell death selectively in cancer cells treated with AuNPs-Gluc, sparing non-tumoral cells. Among the morphologies tested, star-shaped AuNPs exhibited the highest photothermal efficiency. In vivo experiments further substantiated the therapeutic potential, as combined administration of AuNPs-Gluc and laser irradiation significantly suppressed tumor growth ($p < 0.01$). Collectively, these findings highlight the utility of glucose-functionalized AuNPs as effective vectors for targeted PTT in lung cancer, supporting their translational relevance for future clinical applications in advanced-stage disease.

Keywords Advanced stage lung cancer, Gold nanoparticles-based phototherapy, Cancer photothermal therapy

In the last decade, with the advent of targeted therapies, the clinical outcome of patients with non-small cell lung cancer (NSCLC) diagnosed in advanced stages has experienced significant progress[1]. The use of multiple kinase inhibitors for patients with driver mutations, or the administration of first-line immune checkpoint inhibitors (ICIs) for metastatic patients with expression of programmed death receptor ligand 1 (PD-L1), or as adjuvant therapy after chemotherapy treatment in patients with localized disease, has achieved prolonged responses with a significant improvement in survival[2,3]. However, resistance to these new therapeutic options is frequent. In addition, disease prognosis radically decreases when the mediastinal nodes are compromised (nodal metastasis).

[1]Cancer Immunobiology Laboratory, Facultad de Ciencias Biomédicas, Instituto de Investigaciones en Medicina Traslacional (IIMT), CONICET-Universidad Austral, Av. Presidente Perón 1500 (B1629ODT) Derqui-Pilar, Buenos Aires, Argentina. [2]Thoracic Surgery Unit Hospital Universitario Austral, Av. Presidente Perón 1500 (B1629ODT) Derqui-Pilar, Buenos Aires, Argentina. [3]Department of Clinical Oncology, Hospital Universitario Austral, Av. Presidente Perón 1500, (B1629ODT) Derqui-Pilar, Buenos Aires, Argentina. [4]Department of Chemistry 'Ugo Schiff', University of Florence, via della Lastruccia 3-13, Sesto Fiorentino 50019, FI, Italy. [5]Soft Matter Nanotechnology Group, Centro de Investigación Cooperativa en Biomateriales CIC biomaGUNE, Basque Research and Technology Alliance (BRTA), Parque Científico y Tecnológico de Gipuzkoa Paseo Miramón 194, Gipuzkoa, Donostia-San Sebastián 20014, Spain. [6]Instituto de Nanosistemas, Escuela de Bio y Nanotecnologías, Universidad Nacional de San Martín. UNSAM Campus Miguelete, 25 de Mayo y Francia (1650), San Martín, Buenos Aires, Argentina. [7]These authors jointly supervised this work: M. Fernanda Cardinal and Mariana Malvicini. ✉email: fcardinal@unsam.edu.ar; mmalvicini@austral.edu.ar

The 5-year survival rate is more than 90% when diagnosed in the early stages but falls to approximately 24% when the mediastinal lymph nodes are affected[4]. Then, NSCLC remains the primary cause of cancer deaths all over the world[5]. In this context, we need effective tools to eradicate metastatic tumor cells. Nanoparticle-based photothermal therapy has recently been proposed as a low-toxic and feasible opportunity for solid tumors[6]. Gold nanoparticles (AuNPs) have garnered special interest due to their chemical stability and ability to attach molecules to their surface[7]. In addition, the shape or size of AuNPs can be easily tailored to exhibit suitable localized surface plasmon resonances (LSPR) in the near-infrared window (wavelengths between 780 and 3000 nm) according to the chosen laser wavelength. The excitation of these resonances by electromagnetic radiation results in heat release into the environment, cell damage, and induction of cell death by apoptosis.

Gold nanoparticle phototherapy has been successfully used in vivo experimental studies to treat metastatic nodes[8,9]. In these studies, AuNPs administered in mice were irradiated with a low-power infrared laser, which led to cancer cell damage and demonstrated an anti-tumor effect. Then, the accumulation of nanoparticles with LSPR in the near-infrared window absorbs the light, converts energy into heat, and kills tumor cells. As an advantage, because of the low-power laser beam used, photothermal therapy does not damage normal cells nor produce cytotoxicity in healthy tissue like other conventional cancer treatments, such as radio or chemotherapy[10].

AuNPs have shown low toxicity and maintained their biocompatibility when they have been functionalized by attaching polyethylene glycol (AuNPs-PEG) to their surface. More interestingly, AuNPs could also be functionalized with 2-deoxy-D-glucose (AuNPs-Gluc) to increase their concentration in hypermetabolic tumor cells. 2-deoxy-D-glucose enters the cell by diffusion facilitated by GLUT1 glucose transporters, and once inside the cell, it is dephosphorylated by hexokinase to 2-deoxy-D-glucose-6-phosphate (2-DG-6-P). It has been reported that tumor cells have a superior avidity for glucose than normal cells, more hexokinase activity, and less phosphorylase activity[11,12]. Lung cancer cells also have a large avidity for 2-deoxy-D-glucose. Currently, 2-deoxy-D-glucose conjugate with radioactive Fluor (18FDG) is used in Positron Emission Tomography (PET) to detect hypermetabolic tumor sites with high sensitivity for cancer staging. The efficacy of AuNPs for diagnosis and, more importantly, advanced-stage lung cancer treatment has not been demonstrated. In this study, we synthesized AuNPs as spheres, rods, and stars, functionalized them with PEG and 2-deoxy-D-glucose, cultured them with human and murine lung cancer cells, and irradiated them with a suitable laser source. We demonstrated that AuNPs-Gluc plus laser irradiation had an antiproliferative effect and inhibited neoplastic cell viability compared to those that had only been irradiated by laser without nanoparticle administration or those only exposed to AuNPs-Gluc and not irradiated, without affecting non-tumoral cells. Our findings exhibit that the glucose functionalization of AuNPs significantly improves the uptake of nanoparticles by cancer cells and then, after the photothermal effect, selectively induce loss of viability and apoptosis, showing antitumoral efficacy on lung cancer-bearing mice.

Results

Nanoparticles characterization before and after functionalization

The structural and physicochemical characterization of the synthesized nanoparticles was assessed. We prepared gold nanospheres (AuNPs-Sph) (Fig. 1A) with an average diameter of 18 ± 4 nm, as concluded from TEM images, and a localized surface plasmon resonance (LSPR) at 517 nm, determined from the extinction spectrum (comprising both absorption and scattering contributions). We also synthesized gold nanorods (AuNPs-R), obtaining an average particle size of 14 ± 3 nm in width and 60 ± 4 nm in length from TEM images, and with a longitudinal LSPR mode at 946 nm (Fig. 1B). Additionally, we prepared gold nanostars (AuNPs-Stars) of four or five spicules with an approximate spicule length of 41 ± 3 nm on average, and with a final diameter of the star close to 109 ± 4 nm and LSPR of 986 nm. (Fig. 1C). After PEG and 2-deoxy-D-glucose functionalization, all synthesized gold nanoparticles were measured by DLS, and their final hydrodynamic size was 37 ± 1 nm for the spheres, 97 ± 2 nm for the rods, and 71 ± 2 nm for the stars. Zeta potential was slightly negative in every nanoparticle (Supporting Information, Table 1).

Lung cancer cell viability was preserved when AuNPs were functionalized with 2-deoxy-glucose (AuNPs-Gluc)

To select an optimal concentration for testing the efficacy of treatment with AuNPs plus laser irradiation in lung cancer cells, we first evaluated whether AuNPs functionalization showed toxicity and could impact cellular viability. The cytotoxic profile was analyzed using 50, 100, or 200 μg/mL of each form: as-prepared AuNPs, AuNPs-PEG, or AuNPs-Gluc after 3 or 24 hs of culture (Fig. 2). Spheres did not show toxicity when used as AuNPs-Sph-Glu at 50–100 μg/mL but had a toxic effect when used as prepared or AuNPs-Sph-PEG (Fig. 2A; $p < 0.05$ and $p < 0.01$ vs. control at 100 μg/ml; $p < 0.01$ vs. control at 200 μg/mL). We observed that AuNPs-R did not show toxicity when functionalized with glucose (AuNPs-R-Glu) at concentrations of 50–100 μg/mL, while it had a toxic effect when used as prepared or AuNPs-R-PEG at 200 μg/mL (Fig. 2B; $p < 0.001$ vs. control at 50, 100, or 200 μg/mL). Particularly, AuNPs-Stars showed a toxic effect when used as prepared, AuNPs-Stars-PEG, or AuNPs-Stars-Gluc for each concentration when incubated for 24 h (Fig. 2C). Then we incubated cells with 50, 100, or 200 μg/mL AuNPs-Stars for 3 h and observed that cell viability was not affected (Fig. 2D; $p < 0.001$ vs. control at 50, 100, or 200 μg/mL at 24 h; $p < 0.01$ vs. Control at 3 h).

Glucose functionalization of AuNPs improves the uptake of nanoparticles by cancer cells

Next, we examined the potential uptake of functionalized nanoparticles. Cancer cells were incubated with AuNPs-PEG or AuNPs-Gluc at different time points, and the quantity of Au (μg/mL) inside the cells was measured by ICP-MS and qualitatively corroborated by TEM (Fig. 3). We observed that A549 cells incubated with AuNPs-R-Gluc, AuNPs-Sph-Gluc, or AuNPs-Stars-Gluc significantly incorporated more Au particles than A549 cells incubated with AuNPs-R-PEG, AuNPs-Sph-PEG, or AuNPs-Stars-PEG after 3 h of incubation (Fig. 3A; $p < 0.05$

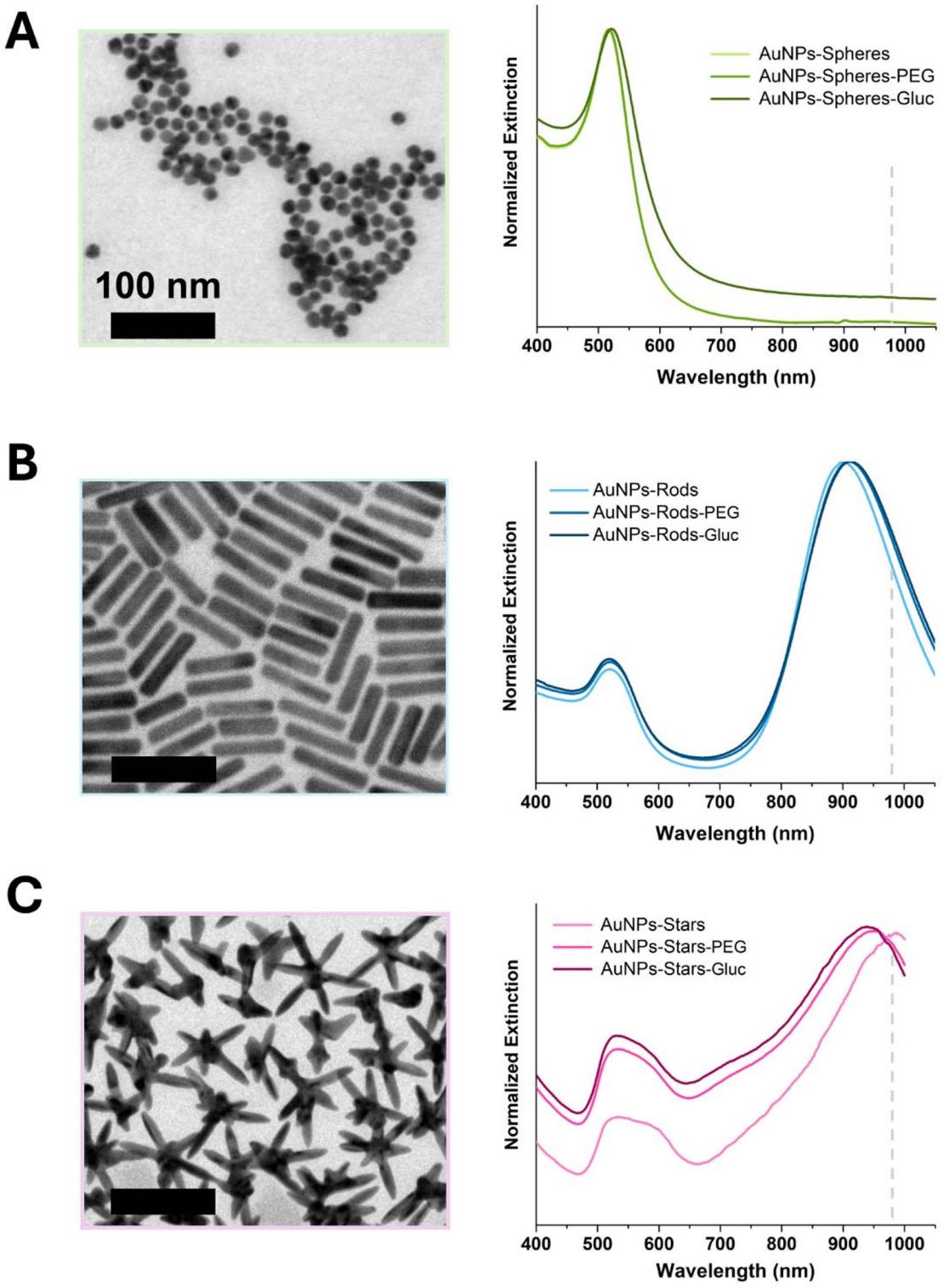

Fig. 1. Gold nanoparticles: (**A**) nanospheres (**B**) nanorods (**C**) nanostars. Left: Representative TEM image, scale bar 100 nm. Right: Normalized extinction spectra at LSPR maxima. Extinction spectra of gold nanospheres are illustrated with green lines, nanorods with blue, and nanostars with pink range lines. In each case, three spectra are graphed: as-prepared colloid (lightest color), after functionalization with PEG (lighter), and after functionalization with glucosamine (darkest respective range color). Grey dashed vertical line at 980 nm, eye guideline of laser line used.

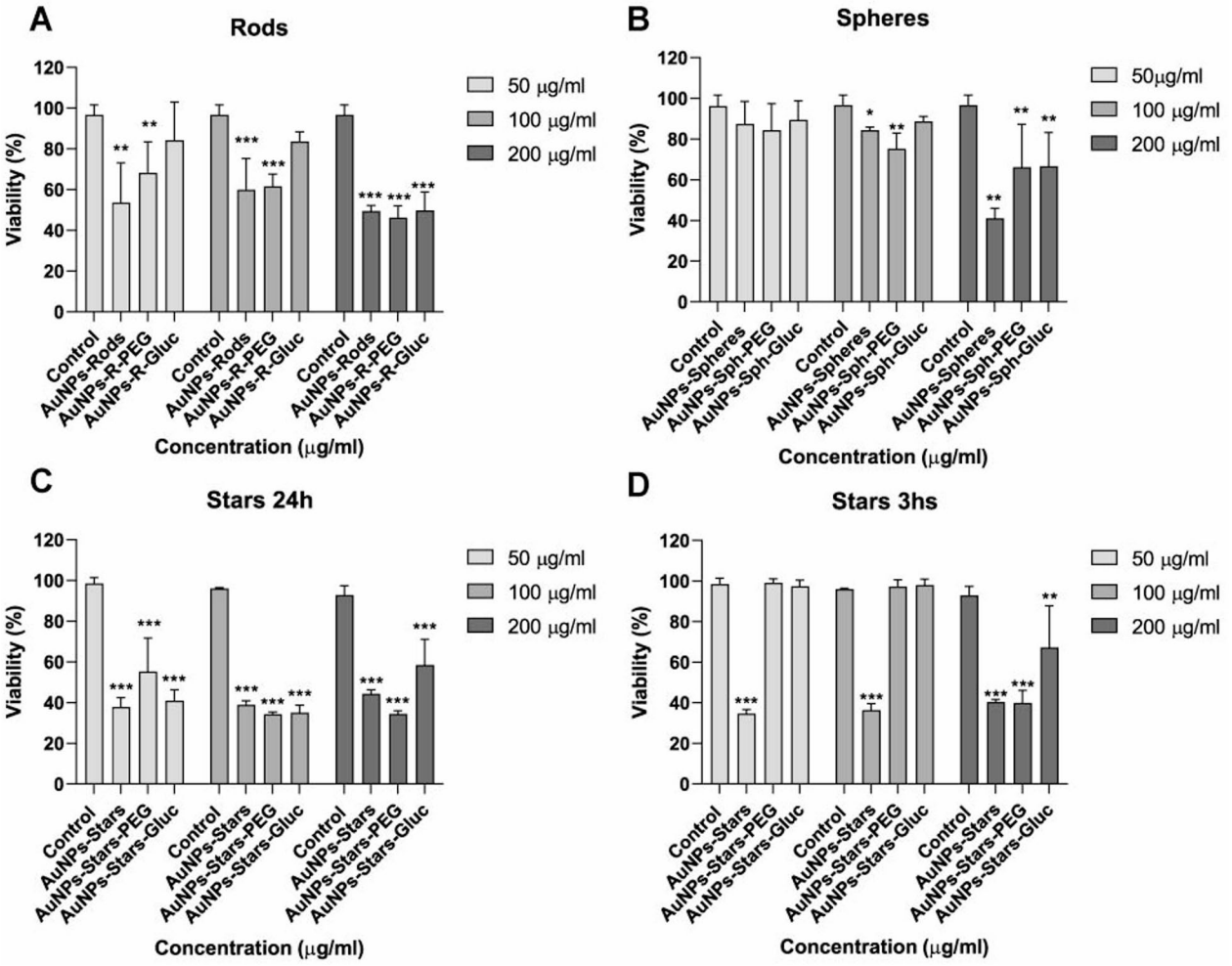

Fig. 2. MTT assay for in vitro toxicity of polyethylene glycol (AuNPs-PEG) or 2-deoxyglucose (AuNPs-Gluc) functionalized nanoparticles. A549 viability was measured after 24 hs of culture with 50, 100, or 200 µg/mL of prepared AuNPs, AuNPs-PEG, or AuNPs-Gluc. (**A**) Rods did not show toxicity when used as AuNPs-Gluc at 100 µg/mL while had a toxic effect when were used as prepared or AuNPs-PEG $^{***}p < 0.001$ vs. control at 50, 100, or 200 µg/mL. (**B**) Spheres did not show toxicity when were used as AuNPs-Gluc at 100 µg/mL while had a toxic effect when were used as prepared or AuNPs-PEG $^{**}p < 0.01$ vs. control at 100–200 µg/mL. (**C**) Stars had shown a toxic effect when were used as prepared, AuNPs-PEG or AuNPs-Gluc when were incubated for 24 h (left) while had no impact on cell viability when AuNPs-Gluc were incubated for 3 h (right) $^{***}p < 0.001$ vs. control (untreated cells) at 50, 100–200 µg/mL at 24 h; $^{***}p < 0.01$ vs. control at 3 h. Data are expressed as mean viability percentage ± standard deviation of quadruplicates.

and $p < 0.01$; AuNPs-PEG vs. AuNPs-Gluc for each type of AuNPs). In addition, we found that AuNPs-R-Gluc, AuNPs-Sph-Gluc, or AuNPs-Stars-Gluc were internalized by A549 cells and located in the cytoplasm, as shown in TEM images (Fig. 3B).

The photothermal effect of AuNPs in solution

To test the capability of converting light energy into the thermal energy of AuNPs, we irradiated them using a 980 nm diode laser at 1 W power. For this purpose, 100 µg/mL AuNPs were resuspended in a mix of 80% oleic and 20% palmitic acids to mimic the mediastinal microenvironment containing fat. Then, the temperature was monitored with a thermocouple. Supplementary Fig. 1A shows the temperature over irradiating time from an initial temperature of 37 °C for all forms of AuNPs. The delta was ΔT = 22.8 °C, 24.6 °C, and 27.4 °C after 2 min of irradiation, for AuNPs-R-Gluc, AuNPs-Sph-Gluc, or AuNPs-Stars-Gluc, respectively, while the control using PBS ΔT = 8.9 °C (Supplementary Fig. 1A). We also tested the optimal time for irradiation, evaluating the effect of the 980 nm laser (1 W) on cancer cell survival (without nanoparticles) at 0.5, 1 and 2 min. Then, we selected 1 W for 1 min as the photothermal approach for the following experiments (Supplementary Fig. 1B).

AuNPs-Gluc plus laser reduces viability and induces apoptosis in human lung cancer cells

To evaluate the efficacy of photothermal therapy using AuNPs-Glu incorporated by cancer cells and then irradiated by laser, we first analyzed A549 cells survival by MTT assay. Figure 4 A shows that AuNPs-R-

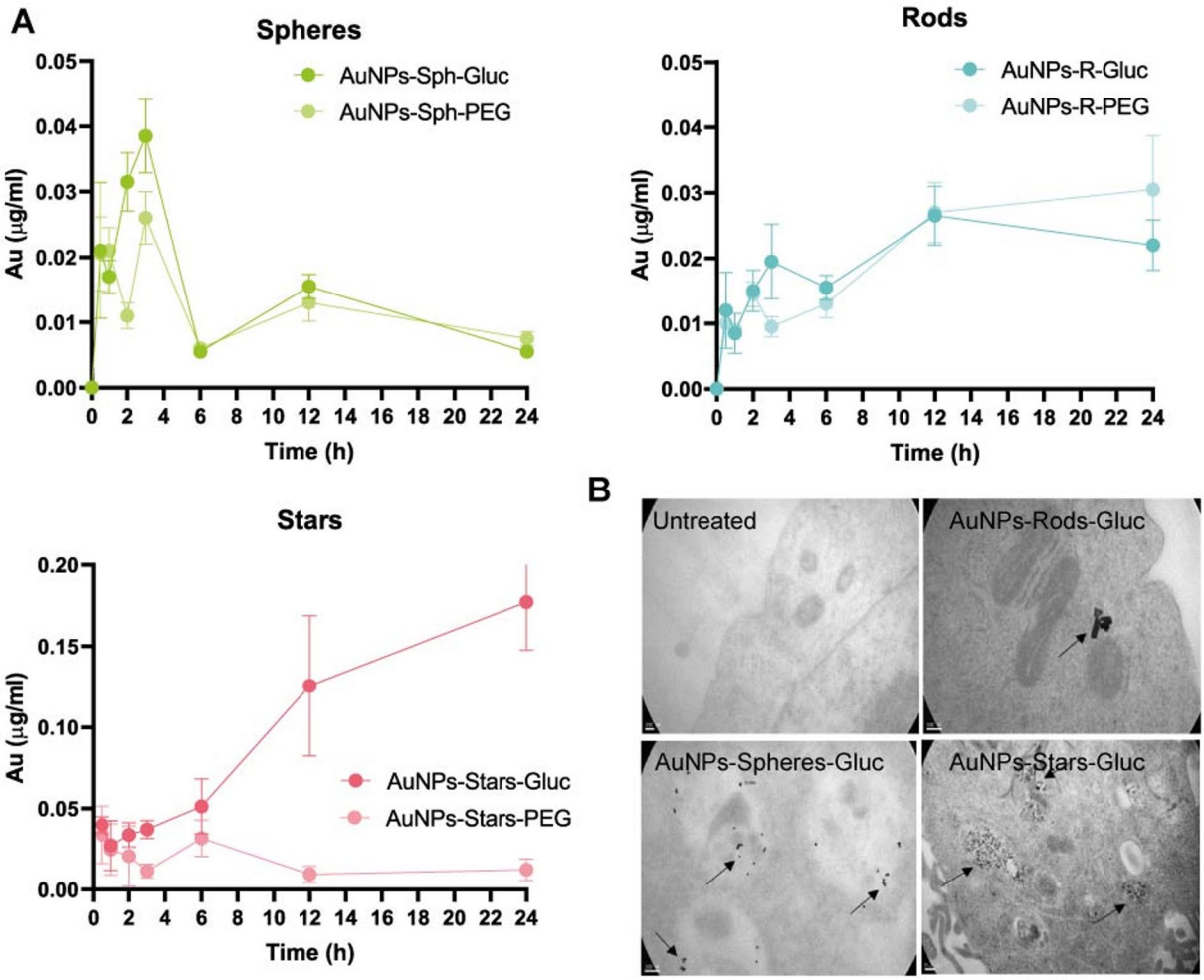

Fig. 3. (**A**) Cellular uptake by ICP-MS quantification of Au (μg/mL) in A549 cell line after incubation with gold nanoparticles functionalized with PEG (AuNPs-PEG; grey) and functionalized with PEG and glucosamine (AuNPs-Gluc; black) at 0.5, 1, 2, 3, 6, 12, and 24 h. *$p < 0.05$ and **$p < 0.01$; AuNPs-PEG vs. AuNPs-Gluc for each type of AuNPs, unpaired T-test. (**B**) Representative TEM image from A549 after 3 h of incubation with Rods, Spheres, and Stars AuNPs-Gluc. Scale bar 100 nm (untreated, rods, spheres) or 0.2 μm (stars).

Gluc + laser, AuNPs-Sph-Gluc + laser, and AuNPs-Stars-Gluc + laser significantly inhibited tumor cell viability: AuNPs-R-Gluc + laser: 74% ± 1 vs. 100% ± 4 AuNPs-R-Gluc; $p < 0.001$; vs. 94% ± 1 laser; $p < 0.001$ and vs. 100% ± 3 untreated A549 cells; $p < 0.01$. AuNPs-Sph-Gluc + laser: 58% ± 8vs. 92% ± 8AuNPs-Sph-Gluc; $p < 0.05$ and vs. 100% ± 2 untreated A549 cells; $p < 0.01$. AuNPs-Stars-Gluc + laser: 59% ± 7 vs. 100% ± 4AuNPs-Stars-Gluc; $p < 0.001$ and vs. 97% ± 3 untreated A549 cells; $p < 0.01$. In addition, AuNPs-Stars-Gluc + laser did not affect Wi38 cells survival (Supplementary Fig. 2, 91% ± 3 viable cells in AuNPs-Stars-Gluc + laser vs. 88% ± 3 in AuNPs-Stars-Gluc; ns; vs. 94% ± 2in laser; ns and 91% ± 3 in untreated fibroblasts; ns).

Considering the cytotoxic activity of AuNPs-Gluc + laser against human lung cancer cells we next examine the capability of photothermal therapy to reproduce its effects in a colony-forming assay. Figure 4B shows that the clonogenic capability measured 15 days post-irradiation was significantly reduced when A549 cells were exposed to our photothermal approach: AuNPs-R-Gluc + laser: 87 ± 35 colonies vs. 294 ± 15 colonies from AuNPs-R-Gluc; $p < 0.05$ and vs. 374 ± 3 colonies from untreated A549 cells; $p < 0.01$. AuNPs-Sph-Gluc + laser: 118 ± 9 vs. 207 ± 3 from AuNPs-Sph-Gluc; $p < 0.001$; vs. 186 ± 16 colonies from laser; $p < 0.01$ and 217 ± 7 colonies from untreated A549 cells; $p < 0.05$. AuNPs-Stars-Gluc + laser: 460 ± 17colonies vs. 843 ± 26 colonies from untreated A549 cells; $p < 0.01$.

One of the proposed mechanisms responsible for the observed antitumoral effects of AuNPs is its ability to induce apoptosis of cancer cells. We also tested tumor cell apoptosis to assess whether our strategy might induce lung cancer programmed cell death. Figure 4C shows that AuNPs-R-Gluc + laser, AuNPs-Sph-Gluc + laser, and AuNPs-Stars-Gluc + laser significantly induced apoptosis of A549 cells measured by Acridine/Orange (A/O) staining ($p < 0.01$) while Wi38 cells remained viable (Supplementary Fig. 2A-B).

Since a more pronounced therapeutic effect was observed with AuNPs-Stars-Gluc + laser, we aimed to confirm this result by measuring Annexin-positive A549 cells by flow cytometry using this strategy. Annexin V,

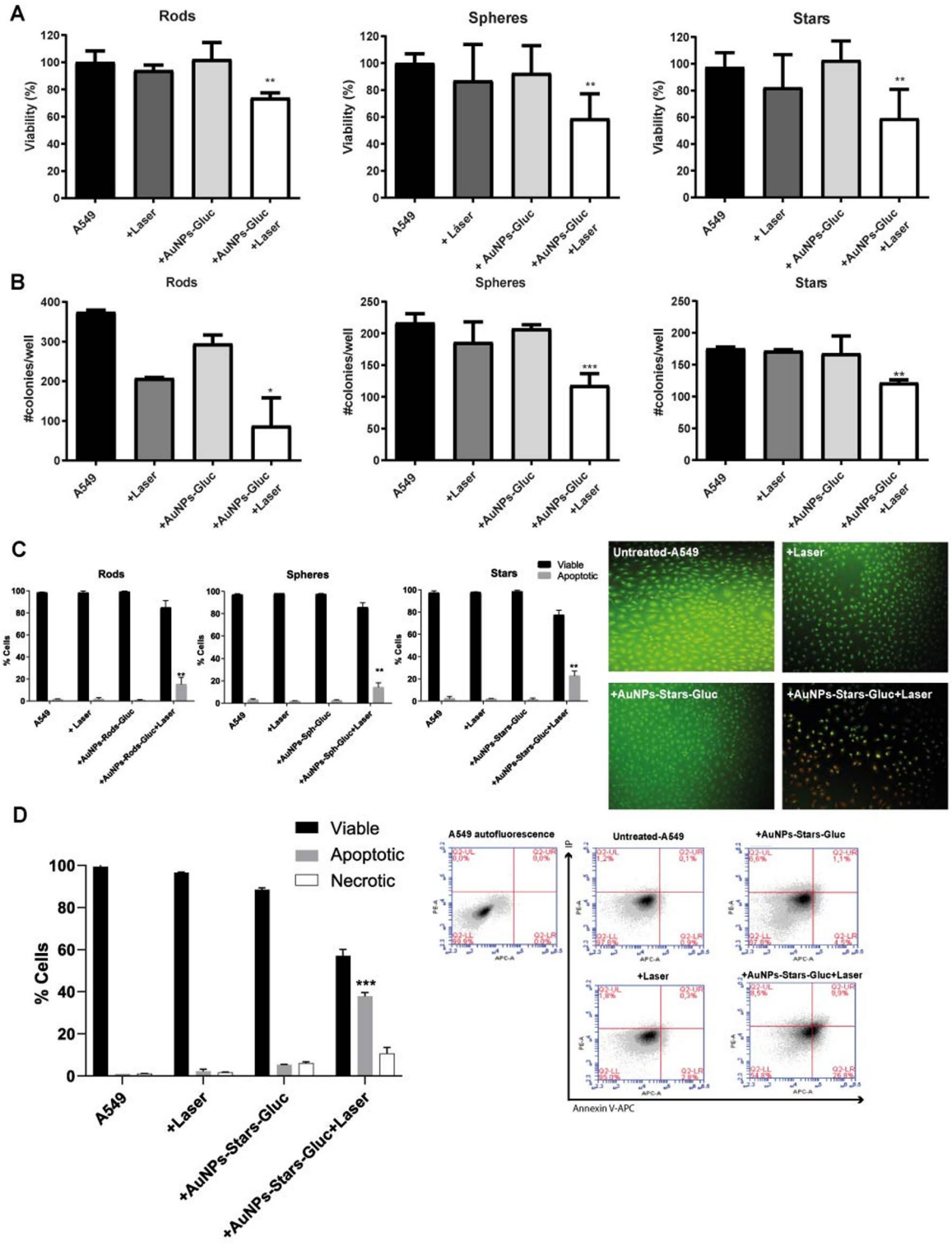

Fig. 4. A549 cells were incubated with Rods, Spheres, or Stars AuNPs-Gluc for 3 hs and then irradiated using a 980 nm laser. (**A**) MTT assay 24 h post-irradiation, (**B**) colony-forming capacity measured 15 days post-irradiation, and (**C**) Acridine/Orange (A/O) staining for apoptotic cells showed low tumor cell viability in AuNPs-Stars-Gluc plus laser-treated cells compared to laser alone or AuNPs-Gluc without irradiation after 24 hs. (**D**) Percentage of apoptotic cells measured by Annexin/PI detection (flow cytometry) is shown. The data are expressed as the Mean ± SEM. $^{*}p < 0.05$ and $^{**}p < 0.01$ A549 vs. A549 + AuNPs-(Rods, Spheres, Stars)-Gluc + Laser. One–way ANOVA and Dunn's multiple comparisons test.

is a protein often used to detect early-stage apoptotic cells due to its ability to bind to phosphatidylserine, which changes its localization on the outer cell membrane when programmed cell death is induced. Figure 4D shows an increased percentage of Annexin-positive (apoptotic) cells when human lung cancer cells were treated with AuNPs-Stars-Gluc + laser in comparison with AuNPs-Stars-Gluc or laser alone and with untreated A549 cells ($p < 0.001$).

Photothermal therapy with AuNPs-Stars-Gluc plus laser also induces death by apoptosis in murine lung cancer and metastatic human lung cancer cells

To demonstrate that the effect on cell survival observed in vitro was independent of A549 cell line susceptibility to the treatment, we set out to evaluate the photothermal therapy effect using AuNPs-Stars-Gluc both on a murine lung cancer cell (LLC1) and a human cell line, obtained from lymph node metastasis (H1299; Fig. 5). In both cases, we observed a significant increase in the percentage of apoptotic cells. Figure 5A shows A/O staining for LLC1 cells: AuNPs-Stars-Gluc + laser: 27% ± 1 apoptotic cells vs. 11.5% ± 0.6 AuNPs-Stars-Gluc; $p < 0.01$ and vs. 4.5% ± 0.6 laser; $p < 0.01$ and vs. 2.7% ± 0.8 untreated A549 cells; $p < 0.001$. Figure 5B shows Annexin positive LLC cells after photothermal therapy measured by flow cytometry: AuNPs-Stars-Gluc + laser: 30.9% ± 1.9 apoptotic cells vs. 21.4% ± 2.0 AuNPs-Stars-Gluc; $p < 0.01$ and vs. 12.6% ± 3.0 laser; $p < 0$. and vs. 17.3% ± 0.1 untreated A549 cells; $p < 0.001$. In addition, in Fig. 5C we confirmed that morphological changes triggered by programmed cell death were also observed in H1299 metastatic cell line: AuNPs-Stars-Gluc + laser: 32.5% ± 5.1 apoptotic cells vs. 3.2% ± 2.2 AuNPs-Stars-Gluc; $p < 0.01$ and vs. 1.0% ± 1.0 laser; $p < 0$. and vs. 2.2% ± 1.1 untreated A549 cells; $p < 0.001$.

AuNPs-Gluc reached the tumor after in vivo administration with no associated acute toxicity and showed a significant antitumoral effect

To assess the in vivo effect of AuNPs-Stars-Gluc + laser, we first administered 100 µg/mL AuNPs-Stars-Gluc endovenously in LLC-tumor-bearing mice C57BL/6 to analyze toxicity and biodistribution at 30 min, 1, 3, 6, and 24 h (Fig. 6). The quantification of Au in tissues by ICP-MS showed that AuNPs-Stars-Gluc reached the tumor at 30 min and remained there after 24 h (Fig. 6A) without acute toxicity, measured by hepatic alanine/ aspartate aminotransferases (ALT/AST) determination in the serum of mice (Fig. 6B).

Then, we assessed the efficacy of irradiated AuNPs-Stars-Gluc (Fig. 6C). After treatment, mice treated with AuNPs-Stars-Gluc + laser showed a significant tumor growth reduction compared to control mice ($p < 0.01$). In addition, mice treated with AuNPs-Stars-Gluc or laser alone progressed similarly to control mice. We observed the same efficacy in male (Fig. 6C, *left*) and female mice (Fig. 6C, *right*). Figure 6D shows that survival of mice receiving AuNPs-Stars-Gluc + laser therapy was significantly higher than the controls ($p < 0.001$; Kaplan Meier; Mantel-Cox log rank test). Microscopic examination of hematoxylin/eosin-stained paraffin-embedded tumor sections obtained 15 days after treatment showed gross areas of necrosis in AuNPs-Stars-Gluc + laser-treated tumors, while no necrotic areas were evident in tumor nodules from animals receiving saline, AuNPs-Stars-Gluc, or laser alone. In addition, tumors treated with the combination showed a marked infiltration of inflammatory cells (Fig. 6E). We also assessed the toxicology profile of AuNPs-Stars-Gluc administration in mice and found that it was well tolerated with no evident signs of clinical, biochemical and hematological toxicity within the studied period of time (Supplementary Fig. 2C-F). Furthermore, we evaluate the stability and biosafety of AuNPs-Stars-Gluc, we carried out UV–Vis spectroscopy measurements of AuNPs-Stars-Gluc in water, PBS buffer and in fetal bovine serum at pH = 7,0 ± 0,1 and pH = 6,5 ± 0,1 as a tumor-like (acidic) environment (Supplementary Fig. 2G).

Discussion

Lung cancer remains a leading cause of cancer-related death globally[5]. For advanced stages, conventional therapies often exhibit limited efficacy and are associated with significant side effects[13–16]. In recent decades, the use of nanoparticles as a new strategy for tumors has led to the development of a novel field of research: nanomedicine against cancer. Compared to conventional therapies, nanoparticles could prevent the occurrence of undesirable effects after being modified to transform into biocompatible[17]. In addition, photothermal therapy using different transduction agents, for instance, nanoparticles, has emerged as a new tumor treatment approach, with some advantages such as precision, high efficiency, and reduced off-target effects[18]. Other authors also demonstrated an antitumor effect using photothermal therapy with agents locally delivered into the tumor[19]. This seems appropriate in locally advanced cancer stages, where it could be possible to administer nanoparticles close to or directly into the tumor mass. Particularly, lung cancer is mostly detected in advanced stages, in which the main problem is distant metastasis and how to manage it[20]. In this scenario, it is necessary to have a treatment capable of reaching all sites where the tumor is localized, avoiding unwanted effects derived from toxicity.

In this study, we have synthesized, characterized, and evaluated the therapeutic efficacy of functionalized gold nanoparticles (AuNPs) for photothermal therapy in lung cancer cells. The gold nanoparticles, including nanospheres (AuNPs-Sph), nanorods (AuNPs-R), and nanostars (AuNPs-Stars), were characterized by their size, morphology, and surface plasmon resonance (LSPR), confirming successful synthesis and functionalization. Synthesis conditions of anisotropic gold particles were successfully tuned to match the resulting LSPR to the excitation laser source wavelength. All colloids remained stable after PEG and 2-deoxy-D-glucose functionalization, as evidenced by the eye, consistent particle size, zeta potential, and extinction spectra. More precisely, all colloids had only minor changes at their extinction spectra before and after each functionalization step. Spheres and rods show minor red shifts of surface plasmon resonances with functionalization steps, tentatively attributed to changes in the refractive index of the surrounding medium due to the PEG polymer. Gold nanostars show minor blue shifts during the functionalization step, which are tentatively attributed to minor spikes reshaping. After functionalization with glucosamine, all colloids have similar (negative) surface

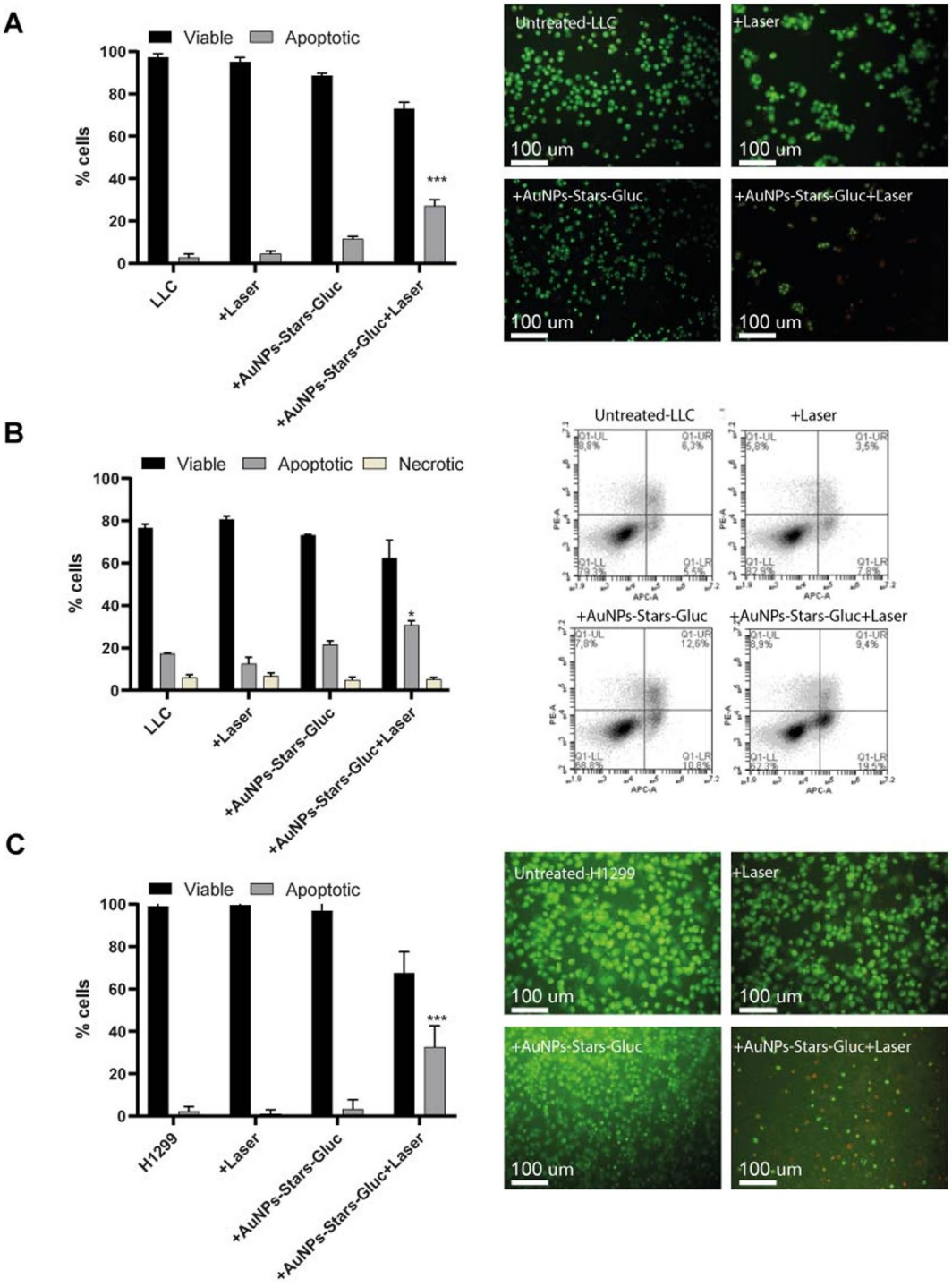

Fig. 5. Photothermal effect of AuNPs-Stars-Gluc on murine Lewis lung carcinoma (LLC) cell line and on metastatic human H1299 cell line. (**A**) Acridine/Orange (A/O) staining for LLC cells was quantified (left) showing low tumor cell viability compared to laser alone or AuNPs-Stars-Gluc without irradiation (right). (**B**) Apoptosis was also measured by Annexin V staining in LLC after 24 h of incubation with AuNPs-Stars-Gluc and laser irradiation $^{*}p < 0.05$ One–way ANOVA and Dunn's multiple comparisons tests. (**C**) A/O staining for metastatic human H1299 cell line also exhibited reduced viability.

potential, regardless of their initial or as-prepared surface potential, ensuring an overall suitability for further biological applications based on previous reports.

Cancer cells possess a higher endocytic capacity than normal cells, largely driven by their elevated metabolic activity[21]. Moreover, structural abnormalities of the tumor vasculature, together with deficient lymphatic drainage, enable AuNPs to accumulate at tumor sites, where they can be internalized by tumor and stromal

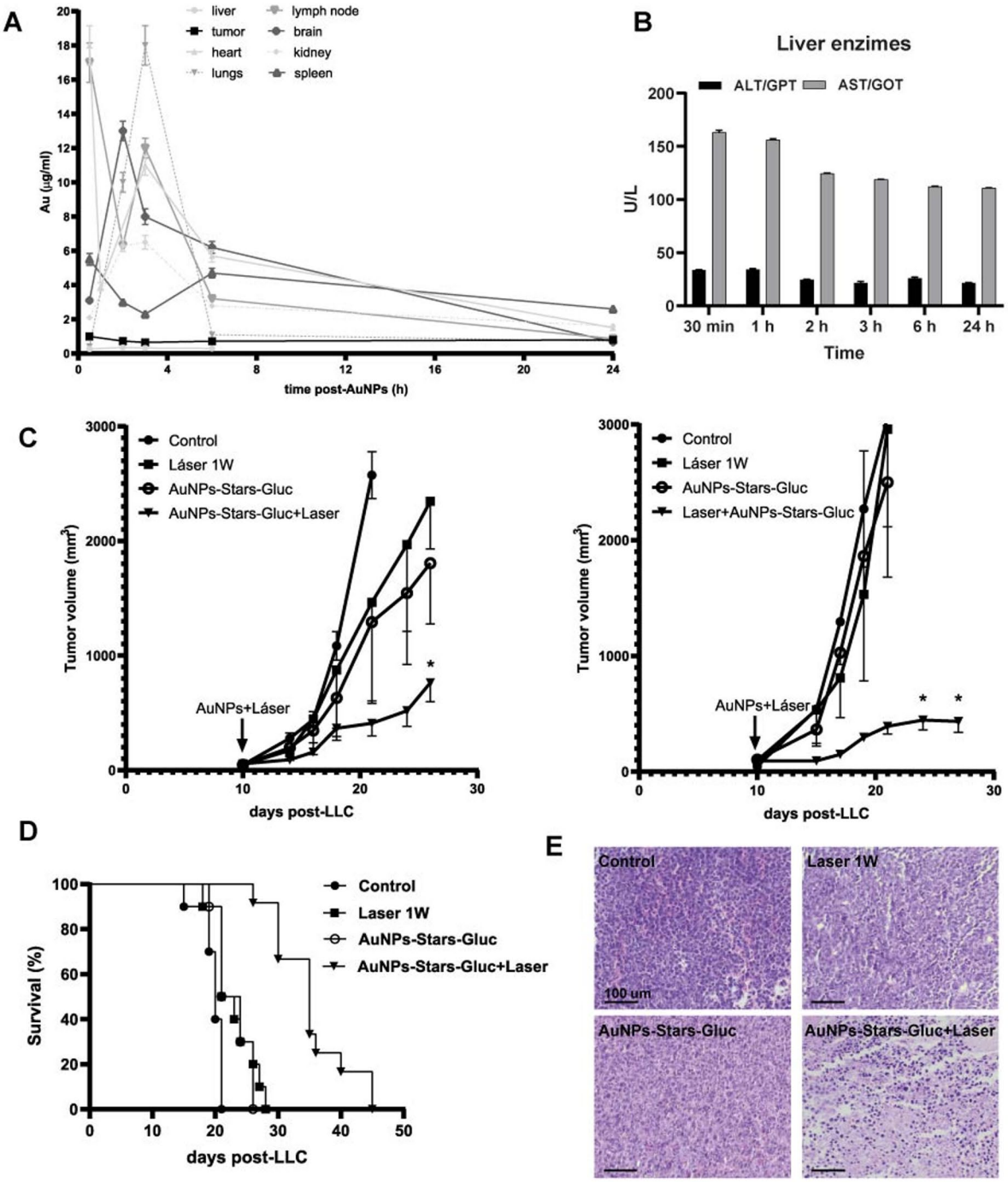

Fig. 6. In vivo effects of irradiated glucose-functionalized AuNPs in a murine model of NSCLC. (**A**) The quantification of Au in tissues by ICP-MS. (**B**) hepatic ALT/AST determination in the serum of treated mice for testing acute toxicity. (**C**) Tumor growth curve. 5-week-old C57BL/6 males (left) or females (right) were used ($n = 5$/group). When the tumors reached 80 mm^3, animals were distributed in sets: the control group received endovenously (e.v) saline; the laser group was irradiated over the tumor for 2 min; AuNPs-Stars-Gluc group received e.v 100 µg/mL nanoparticles; the laser + AuNPs-Stars-Gluc group received e.v 100 µg/mL nanoparticles and was irradiated over the tumor for 2 min, 1 h post-AuNPs-Stars-Gluc administration. $^*p < 0.05$ control, laser, AuNPs-Stars-Gluc vs. the laser + AuNPs-Stars-Gluc One–way ANOVA and Tukey's multiple comparisons tests. No differences were observed between male and female treatment effectiveness. (**D**) Survival of male and female $^{***}p < 0.001$ Mantel-Cox log rank test (AuNPs-Stars-Gluc + laser vs. control). (**E**) Representative hematoxylin-eosin stain from the tumor of all experimental groups. Scale bar 100 µm.

cells through endocytosis. This phenomenon, referred to as the enhanced permeability and retention (EPR) effect, has been widely cited as a basis for nanoparticle accumulation in tumors[22]. Nonetheless, several studies have demonstrated that reliance on passive targeting alone is insufficient, as the heterogeneity of the tumor microenvironment severely limits the reproducibility and efficiency of the EPR effect. Consequently, nanoparticles may also distribute to non-malignant tissues, potentially leading to undesired toxicities[23].

To address these limitations, strategies involving surface functionalization have been proposed to enhance tumor selectivity and reduce off-target effects. Cetuximab-functionalized AuNPs represent a paradigmatic example, demonstrating antiproliferative effects both in vitro and in vivo in low and high EGFR-positive tumors[24]. While promising, this approach restricts therapeutic applicability to a molecularly defined subset of patients, thereby limiting its broader clinical impact. In contrast, our strategy, based on PEGylation to improve nanoparticle stability, combined with glucose functionalization, offers distinct advantages. First, it bypasses dependence on specific receptor expression, expanding potential benefit to a wider patient population. Second, it exploits a metabolic capability of cancer cells, thus enhancing selective uptake by malignant cells over their non-malignant counterparts in the tumor microenvironment.

In our preliminary cytotoxicity studies, we observed that functionalization of AuNPs with glucose (AuNPs-Gluc) did not induce toxicity in lung cancer cells, even at higher concentrations (50–100 μg/mL) and after prolonged incubation (24 h). In contrast, unfunctionalized AuNPs and PEG-functionalized AuNPs exhibited significant toxicity at the highest concentrations tested (200 μg/mL). These findings suggest that glucose functionalization may confer a degree of biocompatibility to the nanoparticles, preserving cell viability and reducing toxicity compared to unmodified AuNPs or those modified with PEG. Interestingly, AuNPs-Stars, regardless of functionalization, showed a higher toxicity profile when compared to nanospheres or nanorods. This could be attributed to the larger surface area and higher surface energy of AuNPs-Stars[25], which may facilitate more effective cellular interaction, though further studies would be required to elucidate the specific mechanisms. Finally, we tested functionalized nanostars for 3 h, observing no toxic effect on cancer cells.

Next, our results demonstrated that AuNPs-Gluc also exhibited enhanced uptake by A549 lung cancer cells compared to AuNPs-PEG. We also observed TEM images confirming internalization. This observation supports again the idea that glucose functionalization facilitates receptor-mediated endocytosis, potentially via the glucose transporter system, which is commonly overexpressed in cancer cells to support their elevated metabolic demands[26]. Additionally, these observations are consistent with previous reports on glucose-coated gold nanoparticles[23,27]. Hu et al., have demonstrated that glucose-coated AuNPs were effective to sensitize acute monocytic leukemia cells and breast cancer cells to X-ray irradiation. On the other hand, Pontico et al. provided the idea that Fluoro-2-deoxy-D-glucose (FDG) functionalized gold nanoparticles are agents with potential for PET imaging and also for radiosensitization. Here, we introduce photothermal therapy as a minimally invasive approach, expanding the applicability of glucose-functionalized AuNPs beyond radiosensitization. Another factor to consider is that protein corona formation on nanoparticles in biological fluids usually detriment designed targeting[28]. From our perspective, overcoming this issue still remains a challenge in the field. Recently, Diloknawarit et al. demonstrated that particles with branches, like gold nanostars, might circumvent protein corona interference[29]. Therefore, we believe that branches in glucose functionalized gold nanostars also play a role in facilitating selective uptake by cancer cells and improve the therapeutic efficacy of AuNPs for subsequent photothermal treatment[30].

We observed a significant photothermal response in glucose-functionalized AuNPs, with a higher temperature increase upon laser irradiation (980 nm, 1 W) compared to the control. This suggests that glucose-functionalized AuNPs, regardless of their shape (nanospheres, nanorods, or nanostars), effectively convert light into heat and can induce hyperthermia. Interestingly, while all AuNP shapes exhibited photothermal effects, AuStars-Gluc showed the most powerful capability, indicating that the particle shape might play a role in enhancing the overall efficacy of photothermal therapy.

Then, we examined the cytotoxicity of irradiated AuNPs-Gluc. We found that AuNPs-Gluc + laser significantly reduced cell viability and induced apoptosis in A549 cells, and AuNPs-Stars-Gluc showed the most pronounced effect. These results were further validated by clonogenic assays, where a marked reduction in colony formation was observed post-treatment. Importantly, the photothermal therapy induced selective apoptosis in A549 lung cancer cells, while normal fibroblasts remained unaffected. Moreover, the efficacy of photothermal therapy was also demonstrated on murine lung cancer cells and human metastatic lung cancer cells, highlighting the potential of AuNPs-Gluc for enhancing photothermal therapy in different lung cancer cells and emphasizing its efficacy in inducing apoptosis. To further assess the translational potential of our findings, we performed in vivo studies using LLC murine lung cancer cells. The results showed that AuNPs-Stars-Gluc were successfully delivered to the tumor site without significant acute toxicity, as confirmed by the absence of changes in hepatic enzyme levels and the histopathological analysis of tissues and organs. Importantly, in vivo treatment with AuNPs-Stars-Gluc + laser significantly reduced tumor growth, supporting the results observed in vitro. These findings highlight the potential of AuNPs-Gluc as an effective therapeutic strategy for lung cancer treatment without systemic toxicity.

The development of nanomedicine has become an opportunity for NSCLC therapy. For their photothermal properties, gold nanoparticles can be administered with irradiation to generate heat, selectively ablating cancer cells[31,32]. Additionally, further combinations of antiangiogenic and/or chemotherapeutic and/or NIR sensitizers, and/or ICIs-based immunotherapy with AuNPs-Gluc offer potentially potent and targeted therapeutic strategies for lung cancer[33,34].

We conclude that our study demonstrates that the successful synthesis and functionalization of gold nanoparticles with 2-deoxy-D-glucose leads to enhanced cellular uptake, allowing photothermal therapy in lung cancer. The therapeutic effects of AuNPs-Gluc in combination with laser irradiation offer a promising strategy for non-invasive cancer treatment. Future work should focus on optimizing the in vivo therapeutic

regime, evaluating long-term safety, and exploring the application of this strategy to develop its clinical potential. Multifunctional nanosystems approach AuNPs-Gluc for targeted and controlled therapeutic interventions, offering a promising avenue for further exploration in lung cancer conduct.

Materials and methods

Preparation and characterization of AuNPs

We synthesized gold nanorods (AuNPs-R), nanospheres (AuNPs-Sph), and nanostars (AuNPs-Stars). For the synthesis of the AuNPs-Sph, we used the Turkevich method[35], obtaining citrate-capped spheres with a diameter of ~ 20 nm, with a localized surface plasmon resonance (LSPR) at 517 nm measured with UV-Vis. We also synthesized AuNPs-R according to El-Sayed et al.'s study[36], obtaining CTAB-capped 14×60 nm rods, with a LSPR at 946 nm. For AuNPs-Stars, we followed the synthesis described by Fabris L et al.[37], obtaining AuNPs-Stars of five spicules with an approximate size of 41 nm long per spicule on average, with a final diameter of the star close to 80 nm and LSPR of 986 nm. Nanoparticles were characterized with transmission electron microscopy (TEM, using a JEOL JEM-1400PLUS system operating at 120 kV) to establish their morphological characteristics and with ultraviolet–visible spectroscopy (UV-Vis) to obtain their optical properties in water. UV- Vis spectroscopy measurements of AuNPs-Stars-Gluc also were determined in Phosphate Buffered Saline (PBS) at pH = 7,0 ± 0,1 and pH = 6,5 ± 0,1 and in fetal bovine serum (FBS) at pH = 7,0 ± 0,1 and pH = 6,5 ± 0,1. Analysis of TEM images was performed with FIJI free software for statistics. Typically, more than 50 nanoparticles of each sample were measured to obtain average dimensions. In addition, we quantified the concentration of atomic gold with inductively coupled plasma mass spectrometry (ICP-MS).

Functionalization of AuNPs The surface of the nanoparticles was functionalized in two steps: (1) PEGilization with HS-PEG5000-COOH (Jenkem Technology USA Inc.) to replace existing ligands, stabilize and turn nanoparticles biocompatible. (2) Addition of glucose by a carbodiimide coupling reaction with N-(3-Dimethylaminopropyl)-N-ethylcarbodiimide hydrochloride (EDC) (Sigma Aldrich)/Nihydroxysulfosuccimide sodium salt (NHS) (Acros Organics) using D-(+)-glucosamine hydrochloride (Sigma). The surface potential (Z-potential) and the hydrodinamic size of each colloid were measured with dynamic light scattering (DLS) using a Zetasizer Nano (Malvern Instruments).

Cells and cell culture

Murine Lewis Lung Carcinoma (LLC), human A549 and H1299 lung cancer cells carcinoma (kindly provided by Prof. Dr. Gabriel Rabinovich and Dra Ada Blinder; Dr. Sergio Moya, and Dr. Elizabeth Martinez respectively) and human lung fibroblasts Wi38 (ATCC-CCL75) were grown in Dulbecco's Modified Eagles Medium (DMEM) or RPMI supplemented with 10% v/v fetal bovine serum (FBS) and antibiotics. Cell cultures were maintained at 37 C in a 5% CO_2 humidified incubator. LLC, A549, H1299, and Wi38 cells were used in different experiments.

Analysis of AuNPs cytotoxicity

The toxicity of functionalized polyethylene glycol (AuNPs-PEG) or 2-deoxy-D-glucose (AuNPs-Gluc) nanoparticles was in vitro measured by the colorimetric MTT assay (Invitrogen). Briefly, 5×10^3 A549 cells were seeded onto 96-well plates in a final volume of 100 µL per well and incubated for 3 h and 24 h with 50 µg/mL, 100 µg/mL, or 200 µg/mL as prepared, AuNPs-PEG or AuNPs-Gluc. Then, the culture medium was replaced with 100 µL of 5 mg/mL 3-(4,5-dime-thylthiazol-3-yl)-2,5-diphenyl tetrazolium bromide. Four hours later, the formazan dye was solubilized and read at 490 nm optical density as previously described.

AuNPs-Gluc uptake by transmission electron microscopy (TEM): A549 cells were incubated with 100 µg/mL AuNPs-Sph-Gluc, AuNPs-R-Gluc, or AuNPs-Stars-Gluc for 3 h. After two washes with PBS, fixed for 15 min, washed, and included in a resin, ultrathin sections were observed under a transmission electron microscope Zeiss EM109T (IBCN-LANAIS-MIE).

AuNPs-Gluc uptake by inductively coupled plasma mass spectrometry (ICP-MS): before ICP-MS analysis, A549 cells were incubated with 100 µg/mL AuNPs-Sph-PEG, AuNPs-R-PEG, AuNPs-Stars-PEG, and AuNPs-Sph-Gluc, AuNPs-R-Gluc, and AuNPs-Stars-Gluc for 0.5, 1, 2, 3, 6, 12, and 24 hs. After 2 washes with PBS, 200 µL of 65% nitric acid was added to each sample, followed by the addition of 100 µL of 30% hydrogen peroxide and brief vortexing. Samples were then incubated in an oven at 70 °C for approximately 2 h. Following incubation, MilliQ water was added to each tube (final nitric acid percentage of ~5%), and all samples were vortexed briefly. Different dilutions were used to ensure all analyses fell within the calibration curves. Final dilutions were then analyzed via ICP-MS.

Gold nanoparticles-based photothermal therapy

LLC, A549, H1299, and Wi38 cells were incubated with 100 µg/mL AuNPs-Sph-Gluc, AuNPs-R-Gluc, or AuNPs-Stars-Gluc for 3 h. After 2 washes with PBS, they were collected with tripsine-EDTA, centrifuged, and resuspended in PBS. Then, cells were irradiated using a 980 nm diode laser (Lumiia SonoBeam) at 1 W (W) power for 2 min.

Cell viability assay and in vitro apoptosis assessment

Briefly, 1×10^6 cells (A549, LLC1, H1299, or Wi38) were plated onto 60-mm dishes and incubated for 3 hs with AuNPs-Gluc. After 2 washes with PBS, cells were collected and irradiated with a 980 nm diode laser at 1 W power for 2 min. Then, 5×10^3 cells were seeded onto 96-well plates in a final volume of 100 µL per well and incubated for 24 h. Cell viability was measured using the colorimetric MTT assay (Invitrogen) described above. Each assay was performed 3 times in quadruplicate.

Morphological changes associated with apoptosis were assessed by acridine orange-ethidium bromide mixture staining (Sigma). Single-cell suspensions were stained with 10 µg/mL of the mixture, and cells were

visualized under a fluorescence microscope. Apoptotic cells were defined as those stained in yellow and showing cytoplasmic and nuclear shrinkage and chromatin condensation or fragmentation. At least 100 cells were counted from 4 independent experiments, and the percentage of apoptotic and necrotic cells was determined and visualized by fluorescence microscopy (Nikon Eclipse E800, Nikon, Buenos Aires, Argentina). The percentage of apoptotic cells was calculated as apoptotic cells (%) = (total number of cells with apoptotic nuclei/total number of cells counted) × 100. Assays were performed in quadruplicate and repeated at least twice. Also, apoptosis analysis was performed on A549 and LLC cells treated with 100 µg/mL AuNPs-Gluc + Laser by flow cytometry at 24 h using an apoptosis detection kit based on annexin-V staining (Biolegend, San Diego, CA). Briefly, murine and human lung cancer cells (1×10^6) were collected with EDTA, washed twice in PBS, centrifuged, and incubated with 5µL annexin-V in a binding buffer at room temperature for 15 min. Cells were vortexed and centrifuged, and the resultant pellets were washed and stained with 1 µL propidium iodide. The percentage of apoptotic cells was analyzed in a FACSAcuri (Becton Dickinson).

Colony formation assay

For colony formation assay, 1×10^6 A549 cells untreated (control) or treated with 100 µg/mL AuNPs-Gluc + Laser were plated onto 60-mm dishes and incubated for 2 weeks before staining with crystal violet. Colonies were quantified under phase-contrast light microscopy. Three independent experiments were performed in duplicate.

Animals

6- to 8-week-old male and female C57BL/6 mice were maintained at our Animal Resources Facilities following the experimental ethical committee and the NIH guidelines on the ethical use of animals. The Animal Care Committee from the School of Biomedical Sciences, Universidad Austral, approved the experimental protocol (code 18 – 05), based on the essential points of the ARRIVE guidelines.

In vivo experimental model

First, C57BL/6 mice were subcutaneously inoculated with 2×10^6 LLC cells into the left flank (day 0). Tumor volume (mm3) was calculated by the formula $\pi/6 \times$ larger diameter $\times$ (smaller diameter)^2 measured with a caliper. When tumors were palpable and reached a volume of approximately 65–70 mm^3 (5–5.5 mm large diameter x 5-mm smaller diameter), mice were inoculated with 100 µg/mL AuNPs-Stars-Gluc intravenously (i.v) to analyze in vivo toxicity by aspartate aminotransferase (AST) to alanine aminotransferase (ALT) levels ratio in the serum (acute liver damage) and biodistribution.

Blood samples were collected from the tail vein using heparinized capillary tubes. Mice were subsequently anesthetized with isoflurane (4–5% for induction, 2% for maintenance in 100% oxygen) via an induction chamber and nose cone. Anesthesia depth was verified by the absence of pedal and corneal reflexes. Then, transcardial perfusion was performed to avoid possible remaining nanoparticles for the subsequent measurement of gold. We used pre-warmed sterile saline infused through the left ventricle, while the right atrium was incised to allow exsanguination. Following perfusion, cervical dislocation was carried out as a secondary physical method. The weight of the mice was an average of 25 g.

We collected samples from the lungs, liver, heart, kidney, spleen, lymph node, brain, and tumor. Then, in other sets of experiments, LLC-bearing mice with approximately 65–70 mm^3 tumors (day 10 after LLC administration), were homogeneously distributed in groups (n = 5–6 per group): (1) (control); or received: (2) 100 µg/mL AuNPs-Stars-Gluc i.v, ; (3) 980 nm diode laser at 1 W for 2 min long, or (4) 100 µg/mL AuNPs-Stars-Gluc i.v + 980 nm diode laser at 1 W for 2 min long, referred as AuNPs-Stars-Gluc + laser. Tumor volume was measured with a caliper 3 times per week, weight was registered once a week, and the maximal tumor size permitted by our Animal Care Committee was not exceeded. The experiment was carried out 2 times. Survival plots were performed when deaths of animals were documented. Samples of liver, spleen and kidney from control mice or mice receiving AuNPs-Stars-Gluc were collected for pathological analysis. Additionally, a set of n = 4 C57BL/6 mice untreated or treated with AuNPs-Stars-Gluc were supervised for 12 days. White cells, platelets, and hemoglobin quantification were analyzed by a cell counter (Sysmex X-N-1000™). Aspartate aminotransferase, alanine aminotransferase, and creatinine levels were measured by standard colorimetric methods (Abbott Alinity C™) The percentage of hemolysis was calculated by the following formula[38]: hemolysis degree (%) = [(100 - Ht) * (free Hb/total Hb)], where Ht: hematocrit (in %), Hb: hemoglobin (in g/dL) and free Hb was obtained by absorbance determination (Abbott Alinity C™).

All procedures were conducted in accordance with our Animal Care Committee guidelines, based on Guide for the Care and Use of Laboratory Animals (NIH, EE.UU.) and the AVMA Guidelines for the Euthanasia of Animals. This study complies with the ARRIVE guidelines for reporting in vivo experiments.

Histopathological analysis

Paraffin-embedded tumor, liver, spleen, and kidney samples were stained with hematoxylin-eosin (H&E).

Statistical analysis

One-way and Two-way ANOVA, Kruskal-Wallis, Mann-Whitney, or Student's t-test (InStat, GraphPad Software) were used to examine the statistical differences between groups. Mice survival was analyzed by a Kaplan-Meier curve and Mantel-Cox log rank test. $P < 0.05$ was considered statistically significant.

Data availability

All data generated or analyzed during this study are available from the corresponding authors on request.

Received: 25 July 2025; Accepted: 15 October 2025

Published online: 20 November 2025

References

1. Yang, S. R. et al. Precision medicine in non-small cell lung cancer: current applications and future directions. *Semin Cancer Biol.* **84**, 184–198 (2022).
2. Tan, A. C. & Tan, D. S. W. Targeted therapies for lung cancer patients with oncogenic driver molecular alterations. *J. Clin. Oncol. Off J. Am. Soc. Clin. Oncol.* **40**, 611–625 (2022).
3. Mamdani, H., Matosevic, S., Khalid, A. B., Durm, G. & Jalal, S. I. Immunotherapy in lung cancer: current landscape and future directions. *Front. Immunol.* **13**, 823618 (2022).
4. Goldstraw, P. et al. The IASLC lung cancer staging project: proposals for revision of the TNM stage groupings in the forthcoming (Eighth) edition of the TNM classification for lung cancer. *J. Thorac. Oncol. Off Publ Int. Assoc. Study Lung Cancer*. **11**, 39–51 (2016).
5. Bray, F. et al. Global cancer statistics 2022: GLOBOCAN estimates of incidence and mortality worldwide for 36 cancers in 185 countries. *CA Cancer J. Clin.* **74**, 229–263 (2024).
6. Okuno, T. et al. Photothermal therapy of tumors in lymph nodes using gold nanorods and near-infrared laser light. *J. Control Release Off J. Control Release Soc.* **172**, 879–884 (2013).
7. Turkmen Koc, S. N., Benam, R., Aral, S., Shahbazi, I. P., Ulubayram, K. & R. & Gold nanoparticles-mediated photothermal and photodynamic therapies for cancer. *Int. J. Pharm.* **655**, 124057 (2024).
8. Oladipo, A. O. et al. A novel treatment for metastatic lymph nodes using lymphatic delivery and photothermal therapy. *Sci. Rep.* **7**, 45459 (2017).
9. Sugiura, T. et al. Photothermal therapy of tumors in lymph nodes using gold nanorods and near-infrared laser light with controlled surface cooling. *Nano Res.* **8**, 3842–3852 (2015).
10. Ungureanu, C. et al. Light interactions with gold nanorods and cells: implications for photothermal nanotherapeutics. *Nano Lett.* **11**, 1887–1894 (2011).
11. Suvarna, S. et al. Synthesis of a novel glucose capped gold nanoparticle as a better theranostic candidate. *PloS One*. **12**, e0178202 (2017).
12. Feng, G., Kong, B., Xing, J. & Chen, J. Enhancing multimodality functional and molecular imaging using glucose-coated gold nanoparticles. *Clin. Radiol.* **69**, 1105–1111 (2014).
13. Higgins, K. A., Puri, S. & Gray, J. E. Systemic and radiation therapy approaches for locally advanced Non-Small-Cell lung cancer. *J. Clin. Oncol. Off J. Am. Soc. Clin. Oncol.* **40**, 576–585 (2022).
14. Oh, S. et al. Locally advanced lung cancer. *Hematol. Oncol. Clin. North. Am.* **37**, 533–555 (2023).
15. Massaro, M. et al. Locally advanced Non-Small cell lung cancer: clinical Outcome, toxicity and predictive factors in patients treated with hypofractionated sequential or exclusive radiotherapy. *Curr. Oncol. Tor. Ont.* **29**, 4893–4901 (2022).
16. Puri, S., Saltos, A., Perez, B., Le, X. & Gray, J. E. Locally Advanced, unresectable Non-Small cell lung cancer. *Curr. Oncol. Rep.* **22**, 31 (2020).
17. Patel, P. & Shah, J. Safety and toxicological considerations of nanomedicines: the future directions. *Curr. Clin. Pharmacol.* **12**, 73–82 (2017).
18. Li, C. et al. Antitumor applications of photothermal agents and photothermal synergistic therapies. *Int. J. Mol. Sci.* **23**, 7909 (2022).
19. Li, X., Lovell, J. F., Yoon, J. & Chen, X. Clinical development and potential of photothermal and photodynamic therapies for cancer. *Nat. Rev. Clin. Oncol.* **17**, 657–674 (2020).
20. Hendriks, L. E. L. et al. Non-small-cell lung cancer. *Nat. Rev. Dis. Primer*. **10**, 71 (2024).
21. Rees, P., Wills, J. W., Brown, M. R., Barnes, C. M. & Summers, H. D. The origin of heterogeneous nanoparticle uptake by cells. *Nat. Commun.* **10**, 2341 (2019).
22. Fang, J., Nakamura, H. & Maeda, H. The EPR effect: unique features of tumor blood vessels for drug delivery, factors involved, and limitations and augmentation of the effect. *Adv. Drug Deliv Rev.* **63**, 136–151 (2011).
23. Pontico, M. et al. 18F-fluorodeoxyglucose (18F-FDG) functionalized gold nanoparticles (GNPs) for plasmonic photothermal ablation of cancer: A review. *Pharmaceutics* **15**, 319 (2023).
24. Qian, Y. et al. Enhanced cytotoxic activity of cetuximab in EGFR-positive lung cancer by conjugating with gold nanoparticles. *Sci. Rep.* **4**, 7490 (2014).
25. Delgado-Corrales, B. J., Chopra, V. & Chauhan, G. Gold nanostars and Nanourchins for enhanced photothermal therapy, bioimaging, and theranostics. *J. Mater. Chem. B.* **13**, 399–428 (2025).
26. Pavlova, N. N. & Thompson, C. B. The emerging hallmarks of cancer metabolism. *Cell. Metab.* **23**, 27–47 (2016).
27. Hu, C., Niestroj, M., Yuan, D., Chang, S. & Chen, J. Treating cancer stem cells and cancer metastasis using glucose-coated gold nanoparticles. *Int. J. Nanomed.* **10**, 2065–2077 (2015).
28. García-Álvarez, R., Hadjidemetriou, M., Sánchez-Iglesias, A., Liz-Marzán, L. M. & Kostarelos, K. In vivo formation of protein Corona on gold nanoparticles. The effect of their size and shape. *Nanoscale* **10**, 1256–1264 (2018).
29. Diloknawarit, B., Schaumann, E. N. & Odom, T. W. High-Curvature features on branched nanoconstructs circumvent protein Corona interference. *ACS Appl. Mater. Interfaces*. **17**, 15187–15195 (2025).
30. Dreifuss, T. et al. Uptake mechanism of metabolic-targeted gold nanoparticles. *Nanomed* **13**, 1535–1549 (2018).
31. D'Acunto, M., Cioni, P., Gabellieri, E. & Presciuttini, G. Exploiting gold nanoparticles for diagnosis and cancer treatments. *Nanotechnology* **32**, 192001 (2021).
32. Domingo-Diez, J. et al. Effectiveness of gold nanorods of different sizes in photothermal therapy to eliminate melanoma and glioblastoma cells. *Int. J. Mol. Sci.* **24**, 13306 (2023).
33. Strozyk, M. S. et al. Multiresponsive nanogel composites for codelivery of antiangiogenic and chemotherapeutic agents. *Chem. Mater.* **29**, 2303–2313 (2017).
34. Forde, P. M. et al. Neoadjuvant nivolumab plus chemotherapy in resectable lung cancer. *N Engl. J. Med.* **386**, 1973–1985 (2022).
35. Kimling, J. et al. Turkevich method for gold nanoparticle synthesis revisited. *J. Phys. Chem. B.* **110**, 15700–15707 (2006).
36. Nikoobakht, B. & El-Sayed, M. A. Preparation and growth mechanism of gold nanorods (NRs) using Seed-Mediated growth method. *Chem. Mater.* **15**, 1957–1962 (2003).
37. Indrasekara, A. S. D. S., Thomas, R. & Fabris, L. Plasmonic properties of regiospecific core-satellite assemblies of gold nanostars and nanospheres. *Phys. Chem. Chem. Phys. PCCP*. **17**, 21133–21142 (2015).
38. de Jonge, G. et al. Interference of in vitro hemolysis complete blood count. *J. Clin. Lab. Anal.* **32**, e22396 (2018).

Acknowledgements

We thank Paula Roselló, Franco Puebla, Anabel Cañete, Santiago Cabrera, and Guillermo Gastón, for their expert technical assistance. We thank Osvaldo Hector Acosta and Mabel Puelles from Laboratorio de Trazas INTI-QUIMICA for providing ICP-MS services. We also thank Quantum Láser SA for providing the Lumiia Laser SonoBeam 980 nm equipment.

Author contributions

Conceptualization JBM, MFC and MM; methodology, JBM, MFC, MF, FP, CAB, PA, MM; formal analysis JBM, MFC, LM, SM, and MM; writing—original draft preparation JBM, MF, MFC and MM; writing—review and editing FP, CAB, MMR, MFC and MM; supervision MFC and MM; funding acquisition JBM, MFC and MM.

Funding

This work was supported by Universidad Austral Convocatorias 2019 and 2022 (MM; JBM); ANPCyT (PICT 2018–3804 and PICT 2021 – 0164 MM; PICT 2018 – 00721 and PICT 2018 – 01126 (MFC)).

Declarations

Competing interests

The authors declare no competing interests.

Consent for publication

All authors have approved the manuscript and agree with its submission to Scientific Reports.

Additional information

Supplementary Information The online version contains supplementary material available at https://doi.org/10.1038/s41598-025-24797-9.

Correspondence and requests for materials should be addressed to M.F.C. or M.M.

Reprints and permissions information is available at www.nature.com/reprints.

Publisher's note Springer Nature remains neutral with regard to jurisdictional claims in published maps and institutional affiliations.